AIAA JOURNAL
Vol. 41, No. 10, October 2003

Electrokinetic Microactuator Arrays and System Architecture for Active Sublayer Control of Turbulent Boundary Layers

Francisco J. Diez* and Werner J. A. Dahm†
University of Michigan, Ann Arbor, Michigan 48109-2140

Results are presented from development of microactuator arrays that function on the electrokinetic principle to provide active control of streamwise sublayer vortical structures in turbulent boundary layers. The electrokinetic microactuator arrays induce volume displacements in the sublayer by electrokinetic pumping under an impulsively applied electric field. These microactuator arrays consist of individual microchannels formed in a substrate and filled with a 1-μm-scale doped porous polymer matrix that provides the required ζ-potential when wetted by the corresponding electrolyte. A system architecture is presented for large dense arrays of such microactuators that provides for greatly reduced control processing requirements within individual unit-cells containing a relatively small number of sensors and actuators. The resulting microactuator arrays have characteristics that make them potentially suited for practical sublayer control on full-scale aeronautical and hydronautical vehicles. Essentially loss-less frequency response of the electrokinetic microactuators has been demonstrated to 10 kHz. Several such microelectrokinetic actuator (MEKA) arrays have been fabricated from a basic three-layer design. A MEKA-5 full-scale hydronautical array, composed of 25,600 individual electrokinetic microactuators with 350-μm center-to-center spacings, arranged in a 40×40 pattern of unit-cells, each composed of a 4×4 matrix of actuators, was successfully fabricated in a 7×7 cm^2 tile in 250-μm-thick Mylar substrate material. Microelectromechanical system design and fabrication processes were used to produce a top layer for the MEKA-5 hydronautical-scale array. DC performance tests indicate that the MEKA-5 array achieves the required flow rates for active sublayer control on hydronautical vehicles with applied voltages of no more than 15–20 V.

I. Introduction

ACTIVE control for drag reduction on aeronautical and hydronautical vehicles is one of the highest-impact applications of microsystems technology and represents one of the longest-standing objectives in the field of fluid dynamics. A reduction in the drag on an air vehicle of just a few percent can translate into large system-wide reductions in fuel weight and operating costs and can provide corresponding increases in vehicle range and payload delivery. Such benefits of microsystems-based drag reduction extend to naval surface and undersea vehicles as well, including ships, submarines, and torpedoes.

It is precisely in the realm of active sublayer control that the underlying physics of the problem at hand and the inherent characteristics of a microsystems-based approach are ideally matched. The thin sublayer in the turbulent boundary layer directly adjacent to the surface of any practical vehicle is one of the most powerful nonlinear systems found in nature, capable of magnifying the effect of small microactuator-induced perturbations into very large changes in the drag acting on the vehicle. Moreover, the exceedingly small length scales associated with flow structures that are naturally present in the viscous sublayer of turbulent boundary layers are ideally matched to microscale actuators. As a result, the inherent problem of matching the length and timescales between microactuators and the physical system being controlled makes the viscous sublayer of a turbulent boundary layer a natural choice for microsystems-based control.

One approach for actively controlling the vehicle boundary layer to achieve drag reduction is to exploit the structure and dynamics of the streamwise vortices that exist naturally in the viscous sublayer. As will be seen next, these sublayer vortices are typically located at distances as small as 10 μm above the vehicle surface, are spaced about 100 μm apart, are roughly 1 mm long, and move past any fixed point on the surface at frequencies up to 100 kHz. These characteristics of the sublayer vortices place stringent limits on the types of actuators that might be suitable for active sublayer control. The present study[1–3] is the first to examine the electrokinetic principle as the basis for a new class of microactuator arrays that are potentially suitable for active sublayer control on real aeronautical and hydronautical vehicles under practical conditions.

A. Background

Early flow-visualization studies (e.g., Ref. 4) first showed the presence of streamwise streak structures in the near-wall region inside the turbulent boundary layer, and subsequent work (e.g., Refs. 5 and 6) revealed their role in the production of turbulence within the boundary layer. These studies found that alternating pairs of counter-rotating streamwise vortical structures at the upper edge of the viscous sublayer were responsible for the "bursting" process by which relatively large amounts of low-speed fluid, in a wall-fixed frame, are suddenly ejected from the near-wall region. These results suggested that control of turbulence production in boundary layers could be achieved by proper manipulation of the near-wall coherent structures.

A number of methods have subsequently been examined to achieve skin-friction reduction by either directly or indirectly controlling the streamwise sublayer structures to interrupt or otherwise alter the near-wall bursting process. These have included passive as well as active means. Among the earliest was the use of long-chain polymer molecules seeded in very low concentrations in the fluid. Their interaction with the sublayer structures produced skin-friction reductions of as much as 80%. More recent work (e.g., Refs. 7–10) has used very low concentrations of self-assembling surfactant ions, which do not suffer from permanent shear degradation, to produce a similar effect. However such polymers and surfactants can only be used in liquid flows. Another class of passive drag-reduction methods has used fine-scale "riblets" (e.g., Refs. 11–14) and shown drag reductions on the order of 8% in laboratory experiments. Other studies, more directly relevant to the present work, have attempted

Received 23 August 2002; revision received 12 February 2003; accepted for publication 14 February 2003.

*Postdoctoral Research Fellow, Laboratory for Turbulence and Combustion, Department of Aerospace Engineering. Member AIAA.

†Professor, Laboratory for Turbulence and Combustion, Department of Aerospace Engineering. Associate Fellow AIAA.

to couple sensors and actuators to provide active control of wall-bounded turbulent flows.[15,16]

The development of microelectromechanical systems (MEMS) technologies over the past decade has opened a new avenue for such active control approaches in the near-wall region of turbulent boundary layers to achieve drag reduction. MEMS fabrication processes allow comparatively inexpensive production of large, dense arrays of microscale wall shear-stress sensors and pressure sensors, typically having length scales of the order of a few hundred micrometers. Such sensor arrays are, in principle, capable of detecting the wall signature of the instantaneous coherent structure pattern in the near-wall region of turbulent boundary layers. Information of this type can, in principle, be used with dense arrays of MEMS-fabricated wall actuators and an appropriate control system to manipulate the near-wall coherent structures and their dynamics in order to interfere with the bursting process. Various attempts to develop sensors, actuators, and control systems to accomplish this goal are discussed in the literature.[15,17–27]

Of particular relevance to the present work, direct numerical simulations by Choi et al. (see Refs. 13 and 18) examined wall shear-stress reduction in turbulent channel flows using local suction and blowing at the wall. Their most successful results used a control approach in which the wall suction or blowing was applied in such a way as to be exactly opposite to the wall-normal component of the velocity at $y^+ \approx 10$, yielding 20–30% reduction in skin friction. That control strategy is now commonly termed "opposition control" (see also Ref. 28). Numerical experiments by Hammond et al.[29] showed the largest wall shear-stress reductions from such an opposition-control strategy based on the wall-normal velocity at $y^+ \approx 15$, with the resulting average drag reduction being about 25%. They suggest that the mechanism for this reduction is the creation of a virtual wall halfway between the detection plane ($y^+ \approx 15$) and the actuation plane ($y^+ = 0$), which reduces the ejection events and thereby interferes with the transport of momentum away from the wall. Rebbeck and Choi[27] have applied such opposition control in wind-tunnel turbulent boundary-layer experiments using wall jets created with piston-type actuators and found changes in the intensity of near-wall bursting events when the jet was issued into the boundary layer.

B. Present Work

The studies noted in the preceding section have shown that active sublayer control of turbulent boundary layers is feasible and have demonstrated several types of actuators suitable for active sublayer control under laboratory conditions. However turbulent boundary layers on aeronautical and hydronautical vehicles are typically at much higher Reynolds numbers and thus involve much smaller length scales and much shorter timescales. Furthermore, actuator arrays on real vehicles will be subjected to nonideal environmental and operating conditions, and thus practical microactuators must be sufficiently robust to permit operation under such conditions. Finally, the power required for large, dense arrays of such microactuators to achieve the desired level of drag reduction must be sufficiently small to provide a significant net reduction in the power requirements of the vehicle.

The present study has examined the electrokinetic principle as the basis for a new class of microactuator arrays that are potentially suitable for active sublayer control on real aeronautical and hydronautical vehicles under practical conditions. The electrokinetic principle involves the interaction between an electric field and mobile ions in the double-layer that forms naturally at the phase interface between a suitable electrolyte and a suitable solid material. Under an applied electric field the mobile ions accelerate as they extract energy from the electric field and then collisionally transfer this kinetic energy to the molecules that make up the bulk of the electrolyte. In this manner an applied electric field can induce bulk motion in the electrolyte. As a result, this electrokinetic flow potentially provides an efficient means for moving comparatively small amounts of fluid on comparatively fast timescales in comparatively small devices. In this study these scaling principles are used together with microfabrication technologies and fundamental considerations of the sublayer structure and dynamics to develop, fabricate, and demonstrate microactuators based on such electrokinetic flow that can meet many of the requirements for active sublayer control in turbulent boundary layers on real vehicles.

In the present electrokinetic microactuator arrays each individual actuator serves as a local volume source, applied over a brief time interval, at the wall. The actuators thus impulsively displace a fixed volume of fluid between the wall and the viscous sublayer to induce lateral displacements in the streamwise sublayer vortices in the manner dictated by the opposition control strategy. Dense arrays consisting of large numbers of such closely spaced electrokinetic microactuators have been designed and fabricated at scales suitable for active sublayer control at real-vehicle conditions. A system architecture is also presented for large, dense arrays of such microactuators that can potentially provide for greatly reduced control processing requirements within individual unit-cells containing a relatively small number of sensors and actuators.

II. Microactuator Performance Requirements

The bursting process associated with streamwise vortices at the outer edge of the viscous sublayer sets the rate of momentum transport from the wall to the fluid and hence the drag that acts on the vehicle. Drag reduction can be accomplished by acting on the streamwise vortices to interrupt or otherwise interfere with this sublayer bursting process. For the present microactuator arrays the individual actuators impulsively produce locally positive or negative displacements to shift the streamwise sublayer vortices along the spanwise direction, as indicated schematically in Fig. 1. To determine the microactuator performance requirements needed to achieve such lateral displacement of the sublayer vortices, this section first reviews essential elements of the structure and dynamics of the near-wall region of turbulent boundary layers. It then uses this information to derive the actuator spacing, frequency, and flow rate requirements necessary to achieve adequate displacement of individual sublayer vortical structures.

A. Structure of Turbulent Boundary Layers

Turbulent boundary layers display a universal structure and scaling in the mean velocity profile under so-called "equilibrium" conditions, which typically apply over much of a vehicle surface. Within the inner layer, owing to the dominance of diffusion, the momentum flux density must be roughly constant at a value equal to the wall shear stress τ_w. All processes within this layer are assumed to be properly scaled with this wall shear stress, the kinematic viscosity ν, the fluid density ρ, and with the distance y above the wall. It is convenient to express this near-wall scaling in terms of the characteristic velocity defined from these quantities equivalently, namely, $u_\tau \equiv (\tau_w/\rho)^{1/2}$, often called the friction velocity, and the characteristic length $l_\tau \equiv \nu/u_\tau$, termed the wall unit or the viscous length scale. The appropriately scaled velocity profile is then $u^+(y^+)$, where $u^+ \equiv u/u_\tau$ and $y^+ \equiv y/l_\tau$.

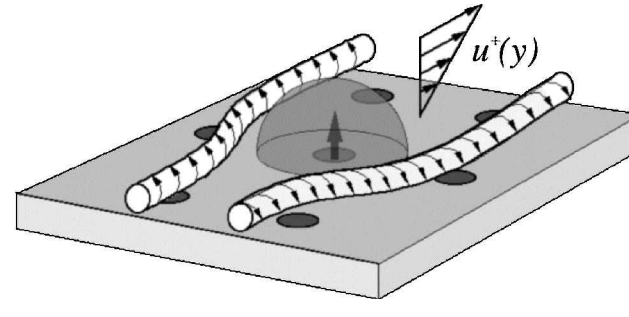

Fig. 1 Idealized notional representation showing the lateral displacement of streamwise sublayer vortices induced by volumetric pumping from an actuator. Note that the Reynolds number associated with the flow issuing from the actuator must be $\mathcal{O}(1)$ or smaller, so that the actuator flow serves as a point volume source to provide effective lateral displacement. At larger Reynolds-number values the flow issuing from the actuator would fundamentally change to become jetlike and would then no longer induce effective lateral displacements.

The streamwise vortices at the outer edge of the viscous sublayer are the key to momentum transport from the inner layer to the outer layer and thus from the wall to the inner layer and thereby determine the drag that acts on the vehicle. These streamwise vortical structures have a spacing in the scaled spanwise coordinate $z^+ \equiv z/l_\tau$ of about $z^+ \approx 100$. The length of these sublayer vortices is typically about $x^+ \approx 1000$, but varies from about 400–1500. The sublayer vortices are thus about 1000 wall units long and are spaced about 100 wall units apart. Because the vortices are located roughly 10 wall units above the wall, they will advect at a speed $u^+ \approx 10$ and thus move over any fixed point on the wall with a frequency of about $f^+ \approx 10^{-2}$.

B. Actuator Spacing, Frequency and Flow Rate Requirements

The electrokinetic microactuator arrays in this study attempt to interfere with the bursting process by impulsively displacing a fixed volume of fluid between the wall and the viscous sublayer to induce lateral displacements of the streamwise sublayer vortices in a manner similar to opposition control. Key performance requirements therefore involve the microactuator spacing, frequency, and flow rate needed to achieve adequate displacement of individual sublayer vortical structures. From the sublayer vortex structure and dynamics just summarized, it is apparent that such actuators must typically be separated about 100 wall units, displace a volume of fluid with an equivalent hemispherical radius of the order of 10 wall units, and achieve a frequency response equivalent to at least $f^+ \approx 10^{-2}$. These performance requirements will depend on the local boundary-layer thickness δ, the local fluid speed U above the boundary layer, the local pressure gradient $\mathrm{d}p/\mathrm{d}x$, and the fluid properties ρ and ν.

Figures 2 and 3 show the resulting microactuator spacing, frequency, and flow rate requirements at four downstream locations along various aeronautical and hydronautical vehicles at four values of the local pressure gradient parameter Π (see also Ref. 19). Among the aeronautical applications the resulting requirements are relatively benign for the unmanned aerial vehicle (UAV), where actuator spacings of several millimeters and frequency response of 100 Hz would be sufficient to act on virtually every sublayer vortical structure. At the other extreme the supersonic fighter and transport aircraft require actuator spacings of 100–200 μm and frequency response of 10–90 kHz. The various hydronautical applications all require microactuator spacings of roughly 300 μm but require frequencies of only about 1 kHz. The equivalent steady volume flow rate, which the microactuators must achieve for each vehicle type, is that needed to impulsively displace the required volume of fluid during the available sublayer vortex passage time. Of key relevance is that the resulting flow rate requirements for hydronautical applications are typically one to two orders of magnitude lower than for aeronautical applications. For essentially all of the hydronautical applications, the equivalent steady flow rate required is in the range of 10 μl/min.

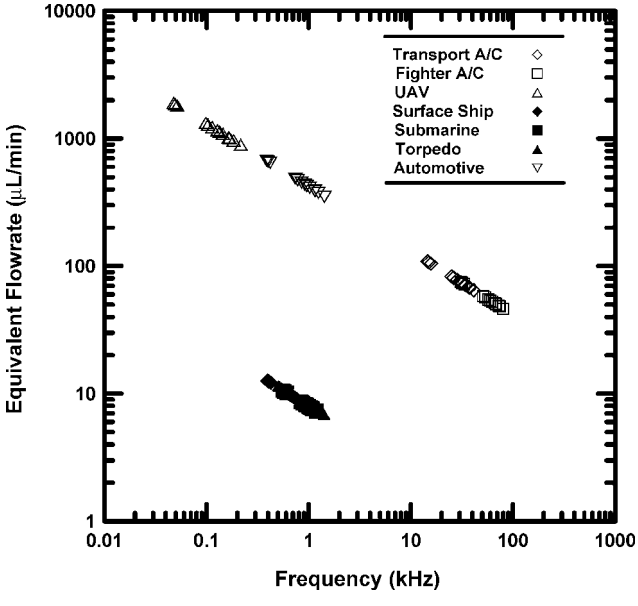

Fig. 2 Equivalent steady volumetric flow rates required for active sublayer control by manipulation of streamwise vortical structures showing results for different aeronautical and hydronautical vehicle types. Hydronautical applications only require flow rates in the range of 10 μl/min, whereas aeronautical vehicle applications typically require one to two orders of magnitude larger flow rates.

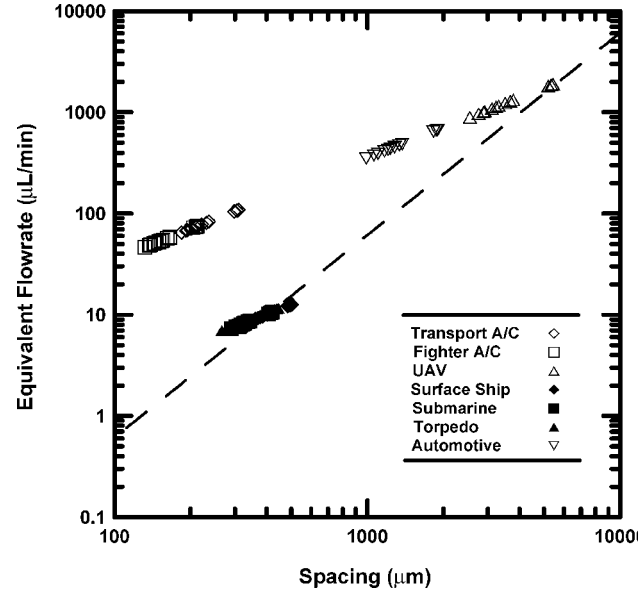

Fig. 3 Microactuator spacing required for active sublayer control by manipulation of streamwise vortical structures showing results for different aeronautical and hydronautical vehicle types, with dashed line showing coupling between microactuator spacing and flow rate, as noted in Sec. II.B, corresponding to simple geometric scaling of any given microactuator design. Increased actuator spacings provide increased area for electrokinetic pumping channels, which in turn provide for larger volume flow rates.

For electrokinetic microactuators intended for use in dense arrays, the maximum flow rate achievable by each actuator is limited by the area per actuator available for the electrokinetic pumping channels, as will be seen in the following. As a consequence, the flow rates are closely tied to the microactuator spacings. This is shown in Fig. 3, where the maximum flow rate achievable is shown as a function of the spacing between individual microactuators within the array. The dashed line shows the result for simple geometric scaling of a given actuator design, for which the flow rate Q increases with actuator spacing l as $Q \sim l^2$. The practical implication is that a microactuator array designed for use in full-scale hydronautical applications can be geometrically scaled up by a factor of 15 to provide the required microactuator array for a UAV-scale aeronautical application. The other aeronautical applications, however, require microactuator arrays that can achieve higher electrokinetic pumping efficiencies, namely, higher values of the equivalent steady flow rate Q per unit microactuator area l^2. For this reason the microactuator arrays developed in this study have been designed for full-scale hydronautical applications. The same array can be directly scaled up, with no increase in per-actuator performance required, for the UAV-scale application.

III. System Architecture for Microactuator Arrays

The small actuator spacing needed for sublayer control on real vehicles implies that large, dense arrays of microactuators must cover key parts of the vehicle surface. For example, the typically 300-μm spacing required in Fig. 3 between microactuators for hydronautical

vehicles of 100 m scale, such as a submarine hull, implies that of the order of 30 billion individual microactuators would be needed to cover the entire vehicle surface. Although most previous studies have focused largely on specific actuator designs or on control processing, it is apparent that the system architecture within which the sensors, actuators, and control processing are implemented is an equally important part of any active sublayer control system. This section describes such an architecture based on a novel unit-cell concept that is sufficiently simple to realistically permit integration of the present electrokinetic microactuators into a complete system for active sublayer control on full-scale vehicles under practical operating conditions. This system architecture provides potentially dramatic reductions in the control processing needed to achieve practical sublayer control.

The difficulty of integrating such a large number of actuators, with a comparably large number of sensors and an appropriate control-processing capability, can be greatly simplified by taking advantage of the inherently local nature of the sublayer structure and dynamics. In particular, the length of the sublayer vortices typically extends over only about 1000 wall units l_τ, and the bursting process occurs between adjacent counter-rotating pairs of these vortices that are typically separated along the spanwise direction by only about 100 l_τ and are typically located about 10 l_τ above the wall. Moreover, the bursting process itself is principally dependent on the separation between the pair of counter-rotating sublayer vortices and is largely independent of the locations and dynamics of other distantly located sublayer vortices. This inherent locality suggests that sublayer control of the turbulent boundary layer over the entire vehicle can be broken down into elementary "unit-cells," the size of which is set by these length scales associated with the sublayer vortex structure. Moreover, if the unit-cells are sufficiently large, then dynamical interactions between them should be comparatively weak in relation to the interactions between sublayer vortices within a given unit-cell. Any such interactions would extend at most to the next adjacent unit-cells, and in a first approximation such cell-to-cell interactions could be neglected altogether. The unit-cells then become fully independent, each with their own sensors, control processing, and actuators. Because the number of sensors and actuators within such unit-cells is then relatively small, the problem of integrating them into a complete control system becomes correspondingly simpler.

The 1000 l_τ average length of the near-wall structures suggests that this is the maximum dimension along the streamwise direction that could be required for such unit-cells. Further reduction is possible by recognizing that incipient bursting occurs far more locally than this, over a smaller length of the sublayer vortex pair. A reasonable limit on the required streamwise dimension of the unit-cells would thus be about 500 l_τ to allow detection of incipient bursting and subsequent actuation to interfere with this process. In the spanwise direction the coherent structures are separated, on average, by about 100 l_τ. Because sublayer control involves acting on pairs of such sublayer vortices near incipient bursting, it appears reasonable that the spanwise dimension of the unit-cell should be large enough to accommodate a given vortex pair and its next adjacent spanwise neighbors. This would suggest that a spanwise dimension of 500 l_τ, equal to the streamwise dimension of the unit-cell, would be sufficient. Based on this reasoning, the fundamental size of the unit-cells in this system architecture is 500 l_τ in both the streamwise and spanwise directions.

The unit-cells are each composed of an $n \times n$ arrangement of elementary sensor and actuator pairs together with local unit-cell processing capability. Given the unit-cell dimensions and the actuator spacings just noted, it is apparent that n will typically be in the range of $4 \leq n \leq 6$, as shown schematically in Fig. 4. Furthermore, the relatively small number n^2 of sensor–actuator pairs in each such unit-cell allows the resident processing capability that connects these sensors and actuators to be greatly simplified. In particular, the number of sensors and actuators is sufficiently small that such true control processing at the unit-cell level can be discarded entirely and replaced by a simple "look-up table" approach. In this case the actuator states are directly implied by the sensor states via a look-up table stored in a simple programmable logic array (PLA)

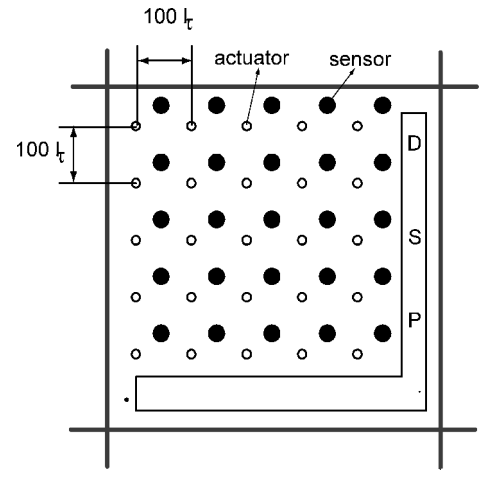

Fig. 4 Basic unit-cell architecture, showing collocated $n \times n$ arrays of typically $4 \leq n \leq 6$ microscale sensors and actuators spaced 100 viscous wall units l_τ apart, with space for unit-cell processing and with common voltage bus lines separating adjacent unit-cells. The relatively small number of sensors and actuators in each unit-cell permits simple look-up table approaches for the unit-cell processing.

in each unit-cell. In this manner on each clock cycle the new sensor states are used to determine the new actuator states, thus eliminating the need for any true processing capability.

Detection of streamwise vortical structures is accomplished by an $n \times n$ array of wall shear-stress sensors collocated with each microactuator in the unit-cell. Many of the usual concerns about shear-stress sensor calibration and accuracy can be relaxed in this system architecture because the role of each sensor is not to measure the wall shear-stress distribution below the vortical structures, but rather simply to identify the presence of a vortical structure just prior to bursting with reasonably high probability of detection. Thus the instantaneous wall shear-stress sensor outputs can be compared to a local running average value obtained from a simple low-pass filter resident in each unit-cell. When the sensor output exceeds a preset multiple of this running average, then the state of the ith sensor in the processing electronics is set to $S_i = 1$ (or to $S_i = \pm 1$ if the sensors have directional capability). Otherwise the sensor state is set to $S_i = 0$.

The complete set of sensor states $\{S_i\}$ for $i = (1, 2, \ldots, n_S)$, where n_S is the number of sensors in each unit-cell, provides the input to the unit-cell processing electronics. Referencing the sensor outputs to a unit-cell-level running average essentially eliminates the need for calibrating each sensor and eliminates difficulties caused by changes in the vehicle speed and attitude or by the particular location of the sensor-actuator pair on the vehicle. Sensor drift over timescales significantly longer than the averaging time thus becomes irrelevant, and sensor accuracy does not need to be high because the sensor output is thresholded in the manner already described.

Because all interactions between the sensors and actuators occur at the unit-cell level, each unit-cell contains its own independent processing capability. Because of the relatively small unit-cell size that the sublayer bursting process allows, it might be possible to greatly reduce the required sensor capabilities and unit-cell processing capabilities. The role of the local unit-cell processing is to use the n_S sensor states $\{S_i\}$ on each clock cycle to determine the n_A actuator states $\{A_i\}$, where $A_i = +1$, 0, or -1 corresponds respectively to positive volume flux (blowing), zero volume flux, or negative volume flux (suction). The actuators are not modulated; they are either on (± 1) or off (0). Thus the voltage of the top-layer electrode for each actuator is set to $A_i V_{\text{ref}}$, where V_{ref} is the voltage of the common power bus that runs between the unit-cells. The processing circuit thus effectively acts as a three-state bridge between this power bus and the electrode contact for each of the microactuators in the unit-cell.

The set of sensor states $\boldsymbol{S} = \{S_i\}$ implies a set of actuator states $\boldsymbol{A} = \{A_i\}$. Functional approaches of the type $\boldsymbol{A} = f(\boldsymbol{S})$ can be appealing in their generality and rigorous connection to control theory, but are likely to require significantly more processing capability than can be readily accommodated within such unit-cells. Moreover, such an approach would overlook the fact that the physics of the sublayer structures greatly restrict this functional dependence and thus provide opportunities for further simplification. Because the processing is purely local at the unit-cell level and the unit-cell size can be made relatively small, it might be possible to use a simple look-up table approach that eliminates the need for complex processing. Such a look-up table can be implemented at various levels of approximation. The simplest is to make use of the nominally streamwise structure of the sublayer vortices and thereby reduce the number of spatial dimensions in both the sensor and actuator arrays to just one. This can be done by logically grouping the n_S sensors in the unit-cell into n_{CS} columns along the streamwise direction and then obtaining a single sensor column state CS_i for each column (e.g., by a majority rule among the sensor states $\{S_i\}$ within the column). Similarly, the n_A actuators are grouped into streamwise columns, and a single actuator column state CA_i is used to drive all of the actuators in that column. This reduces the logic circuit requirements to setting the n_{CA}-element column state vector $\{CA_i\}$ from the n_{CS}-element column state vector $\{CS_i\}$ and can be done by the programmable logic array shown schematically in Fig. 5. In that case the logic array can contain a set of matrix coefficients that provide the actuator state vector for any given sensor state vector.

For the relatively small number of columns provided by the unit-cell architecture, the number of possible sensor column vector combinations might be sufficiently small that each of the appropriate actuator column vectors can be explicitly determined from simple model-based considerations. Alternatively, irrespective of whether the unit-cell processing is to be done in one or two spatial dimensions, because the look-up table remains static and is the same for all unit-cells, it can be generated from a detailed simulations or experiments. This can be done, for example, by an automated neural net approach that continuously evolves to determine a look-up table, which minimizes the wall shear stress within a unit-cell from discrete thresholded sensor inputs S_i. Such an approach to generating the look-up table might be able to incorporate recent advances in applications of control theory to wall shear stress reduction.

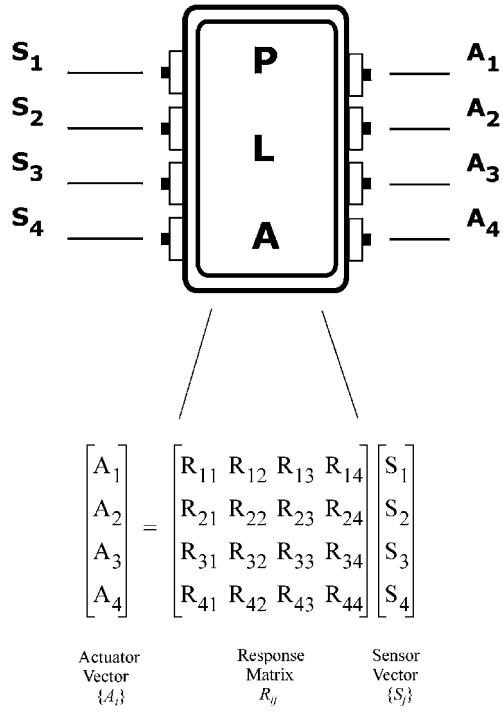

Fig. 5 Minimal PLA content in each unit-cell, giving actuator state vector $\{A_i\}$ as a linear function of the sensor state vector $\{S_i\}$ for a restricted subset of possible sensor states. Several such response matrices R_{ij}, each applicable for such a restricted set of sensor states S_i, would be contained within the PLA on each unit-cell.

IV. Electrokinetic Actuation

The electrokinetic microactuators function on the basis of the electrokinetic effect.[30–32] The present study is the first to examine its potential advantages as the basis for a class of microscale actuators suitable for active sublayer control in turbulent boundary layers at full-scale vehicle operating conditions.

A. Double-Layer Formation

The electrokinetic effect occurs at the interface between a solid polymer and an electrolytic fluid, where an ionic double layer forms naturally at such an interface. It is the presence of this double layer and its interaction with the imposed electric field that is central to the electrokinetic flow principle on which these microactuators are based and thus to the operating performance which these microactuator arrays can achieve. The double layer forms as a result of the interface charge that arises from ionization of surface acid or basic groups in the solid phase. For the present electrokinetic microactuator arrays the solid phase consists of a porous polymer doped with sulfonic acid groups of the form R-SO_4H, where R can represent any of a number of different organic structures. The ionization of this acid that results from contact with an electrolyte produces surface sulfate ions of the form R-SO_4^-. Such ionization of the surface acid or base groups leaves an excess negative charge on the surface and an excess positive charge in the liquid. The interaction between the wall charges and the oppositely charged counterions in the electrolyte buffer gives rise to a so-called double-layer structure near the wall. This double-layer structure of the counterions in the vicinity of the wall is comprised of an immobile inner layer and a diffuse outer layer. The counterions within this diffuse outer layer are free to drift under an applied electric field, and it is their motion in the presence of an applied field that forms the basis of the electrokinetically induced flow.

B. Electrokinetic Pumping

The Navier–Stokes equation can be used to obtain the detailed outer-layer structure and the resulting electrokinetic pumping that it induces under the influence of an applied electric field.[32,33] Under steady-state conditions for the axisymmetric flow that results in an infinitely long capillary or pore channel this can be written in polar coordinates as

$$\mu \frac{1}{r}\frac{\mathrm{d}}{\mathrm{d}r}\left(r\frac{\mathrm{d}v_z}{\mathrm{d}r}\right) = -P_z - E_z\rho(r) \tag{1}$$

where P_z is the pressure gradient $-\mathrm{d}p/\mathrm{d}z$ and E_z is an axial electric field on the net charge density in the double layer. The charge density $\rho(r)$ at a distance r from the surface can be written using the Boltzman distribution and simplified for small potentials $\psi < 50$ mV above that of a solution containing uniformly distributed ions.[34] Thus, for an electrolyte with monovalent ions the charge density is

$$\rho(r) = -2ne^2\psi/kT \tag{2}$$

The double-layer thickness is then given by the Debye length

$$1/\kappa = (\varepsilon kT/2ne^2)^{\frac{1}{2}} \tag{3}$$

where ε is the permittivity of the electrolyte, k is the Boltzmann constant, T is the temperature, and e is the ionic charge. Typical values of $1/\kappa$ for aqueous electrolyte solutions can range from 0.5 to 1000 nm and decrease with increasing ion concentration n.

For the present electrokinetic microactuators no pressure gradient P_z is applied, and the flow results entirely from the applied electric field E_z. Solving Eq. (1) under these conditions, the velocity v_z outside the double layer can be obtained as

$$v_z(r) = -\Omega E_z \tag{4}$$

where $\Omega \equiv \varepsilon\zeta/\mu$ is the ionic mobility, with $\zeta \equiv \psi(r = w)$, where w is the radius of the channel.

For channels with radius much larger than the double-layer thickness ($\kappa w \gg 1$), the volume flow rate Q obtained is by integrating v_z as

$$Q = \pi w^2 \Omega E_z \tag{5}$$

These scalings are for a single channel. For a channel of length L and radius R consisting of $(R/w)^2$ individual pores each of radius w, the flow rate in Eq. (5) becomes

$$Q = \pi R^2 \Omega E_z \tag{6}$$

with the resulting flow speed $U = Q/\pi R^2$, and the force F achieved in a plugged channel becomes

$$F = 8\mu\Omega (R/w)^2 E_z L \tag{7}$$

Note in Eq. (6) that the flow rate achieved is independent of the pore radius w, but the force in Eq. (7) increases as the pores are made smaller. This indicates that by fabricating electrokinetic channels with sufficiently small pores, it might be possible to achieve flow rates adequate to meet the flow rate requirements for sublayer control while achieving sufficiently high pressures in any plugged actuators to allow these to unplug themselves.

C. Hydrodynamic Models of Frequency Response

The ultimate frequency response limits of unsteady electrokinetic processes have not been fundamentally examined in the literature, however assuming that capacitances are properly managed the limiting process is inertial damping by the electrolyte flow within the electrokinetic channels. Quantitative estimates of this inertial damping limit in the electrokinetic flow within a typical pore of radius w can be obtained by a simple hydrodynamic model. This model applies when the electrokinetic double-layer thickness κ is much smaller than the pore radius w, as is typically the case in practical applications. The motion induced in the double layer by either an impulsively applied electric field or by a sinusoidally oscillating applied field is then equivalent, respectively, to Stokes's first or second problem for the flow induced by viscous diffusion above a moving wall. The "wall" in this case is the thin double layer, and viscosity acts to diffuse the induced motion within it throughout the electrolyte across the pore.

Stokes's first problem corresponds to the case where the wall is impulsively set into motion, as would apply for an impulsively applied electric field. The resulting fluid motion is confined to a Stokes layer with thickness $\delta \approx (\nu t)^{1/2}$ adjacent to the wall within which viscous diffusion is able to induce flow. Defining the steady flow rate $Q_{DC} = \pi w^2 U_{eq}$ achieved by a steady (dc) applied voltage across the electrokinetic driver channel, the ratio of the unsteady to steady flow rates is given by

$$Q(t)/Q_{DC} \approx \sqrt{\nu t}/w \tag{8}$$

Assuming an aqueous electrolyte with kinematic viscosity comparable to that of water ($\nu \approx 10^{-6}$ m^2/s) and $w \approx 1$ μm pore sizes, this would indicate that the unsteady flow rate will remain essentially the same as the steady flow rate up to applied frequencies of the order of 10^6 Hz. As a result, essentially no loss of electrokinetic pumping performance will be seen until the frequency of the applied electric field approaches 1 MHz.

Stokes's second problem corresponds to the electrokinetic flow induced by a sinusoidally varying applied electric field. We can define the flow rate Q'_{AC} that results during each volumetric displacement "stroke" of the actuator as Q'_{AC} and the flow rate that would result during the same time by steady electrokinetic pumping as Q'_{DC}. Inertial effects in the induced flow are negligible when "quasi-steady" performance is achieved, namely, when $Q'_{AC}/Q'_{DC} \approx 1$. From the Stokes solution the ratio of these two flow rates becomes

$$Q'_{AC}/Q'_{DC} \approx \sqrt{2\nu/\omega}\,\big/\,w \tag{9}$$

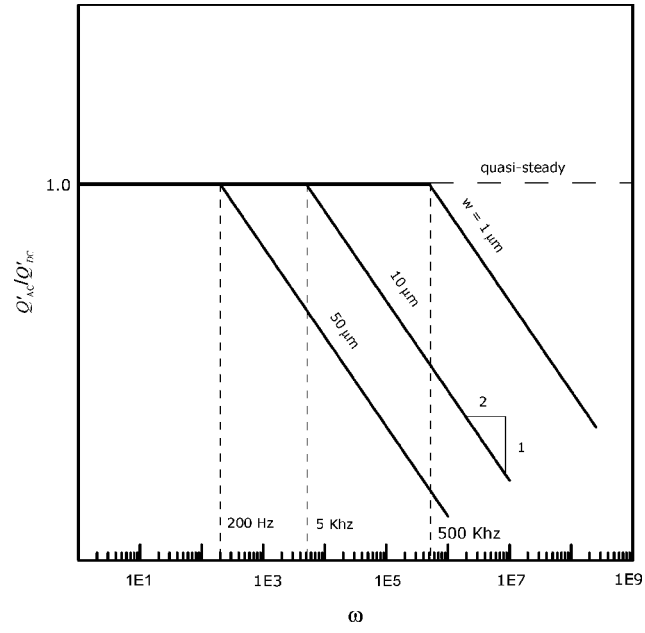

Fig. 6 Ratio of Q'_{AC} to Q'_{DC} from Eq. (9) for any sinusoidal component of frequency ω in an unsteady applied electric field. For $Q'_{AC}/Q'_{DC} \approx 1$ volumetric displacement achieved by electrokinetic pumping is in the quasi-steady limit with no losses caused by inertia effects. For 1-μm pore sizes as in Sec. V, roll-off produced by inertial effects does not begin until frequencies above 500 kHz.

From relation (9) the cutoff frequency across which the actuator response changes from quasi-steady performance to a frequency-limited roll-off can be inferred, as shown in Fig. 6. Again assuming an aqueous electrolyte with kinematic viscosity comparable to that of water, this indicates a cutoff frequency of the order of 500 kHz for 1-μm pores. For the porous polymer matrix used to fabricate the arrays in this study, the average pore size is roughly 1 μm, and this would suggest essentially loss-less frequency response up to around 500 kHz. These considerations indicate that it should be possible to meet the frequency response requirements for all of the vehicle types in Fig. 2 with electrokinetic microactuators having typically 1-μm pore radii in the electrokinetic channels.

V. Electrokinetic Microactuator Array

A. Three-Layer Design

Prior studies have developed processes for creating porous polymer matrix structures, with 1-μm-scale pore sizes, that can be suitably doped to provide electrokinetic flow.[35,36] These provide the basis for a fundamental three-layer design of electrokinetic microactuator arrays. This three-layer design, shown schematically in Fig. 7a, uses a center layer containing individual electrokinetic driver channels formed in an appropriate substrate material and filled with this porous polymer matrix structure.[37] The porous matrix structure can be readily created throughout these individual channels by introducing the polymer in liquid form immediately after mixing its two principal constituents. Dopants previously added to these principal polymer constituents provide the desired acidic or basic groups on the solid surface; the particular choice and concentration of dopants depends on the intended electrolyte and the desired zeta potential. The center layer in this three-layer design consists only of the individual electrokinetic driver channels filled with such porous polymer matrix structures, as shown in Fig. 7a.

Once the curing process in the center layer is completed to produce the porous polymer, the resulting structure can be readily wetted with electrolyte by simple capillary wicking action. Continual contact with the electrolyte, and thereby continual wetting of the entire porous matrix throughout each individual actuator channel in the center layer, is provided by a common electrolyte reservoir in the bottom layer, as shown in Fig. 7a. Because each unit-cell

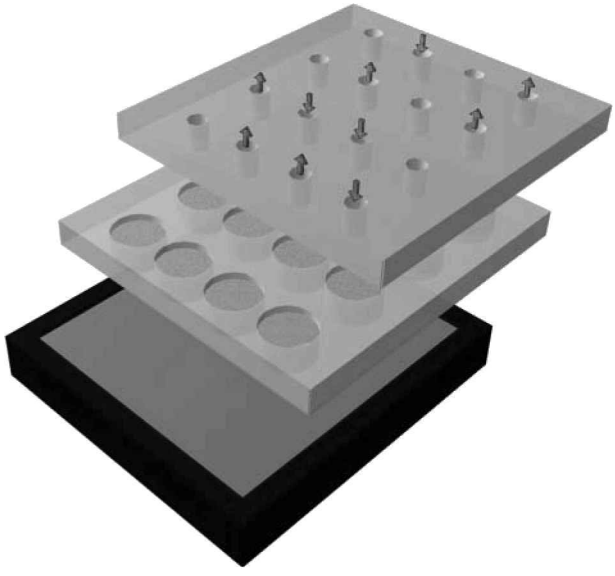

Fig. 7a Basic three-layer design of MEKA electrokinetic microactuators arrays in Sec. V, with center layer containing porous polymer matrix structure.

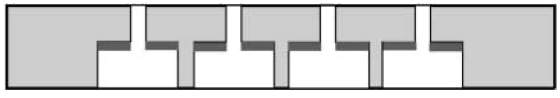

Fig. 7b Typical cross-sectional view of the top-layer structure showing cavity, electrode, and channels for each actuator.

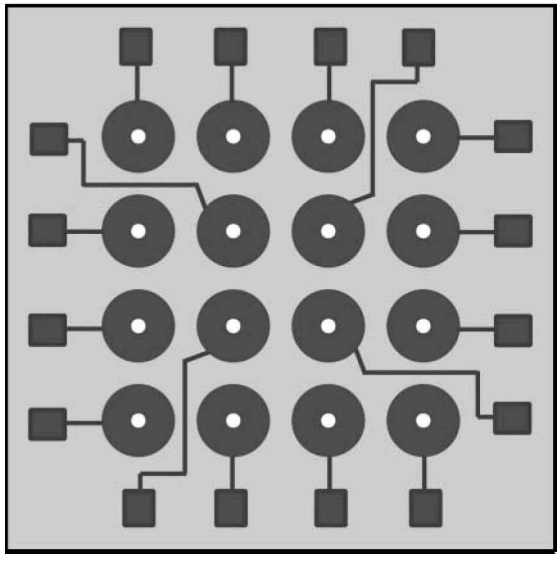

Fig. 7c Electrodes and leadouts to unit-cell contacts.

acts as a zero-net-displacement entity, a fixed amount of electrolyte is maintained within each unit-cell or, alternatively, within each tile.

Note that no electrolyte is discharged from the unit-cell; the electrokinetic flow induced in the electrolyte when an electric field is applied across any individual center-layer channel serves only to displace the working fluid (ambient fluid) from the top layer. This top layer, shown in Fig. 7, includes a nozzle directly above each actuator channel in which working fluid is displaced by pumping of electrolyte in the center layer and issues through the top surface. In cases where the electrolyte must be separated from the working fluid, as would typically be the case for hydronautical applications, a thin layer of flexible membrane material would be sandwiched between the center and top layers. The top layer also contains a circular disk electrode for each actuator channel, with leadouts to connectors near the periphery of the unit-cell shown in Fig. 7c. These are connected with either positive or negative polarity by the unit-cell control circuitry to the common voltage bus that runs between unit-cells. This provides for a positive or negative electric field along each actuator channel between the top-layer electrode and the common electrode in the electrolyte reservoir in the bottom layer, producing positive or negative pumping of the electrolyte, and thereby producing positive or negative displacement of the working fluid from the top surface.

B. MEKA-5 Actuator Array

Several microelectrokinetic actuator (MEKA) arrays have been fabricated from the three-layer design shown in Fig. 7. This basic three-layer design allows for dense arrays comprised of large numbers of such actuators to be fabricated in thin conformally applicable tiles that can accommodate the unit-cell system architecture described in Sec. III and that might in principle be easily applied to the surface of real vehicles. A complete description of the five successive generations of elements of these electrokinetic microactuator arrays developed is given in Diez-Garias.[37] This has led to the MEKA-5 actuator array, shown in Fig. 8, which demonstrated fabrication of a full hydronautical-scale array of electrokinetic microactuators and their integration with a top layer containing the basic unit-cell structure and all electrical leadouts required for actuation. The array was fabricated in a 7×7 cm^2 tile in 250-μm-thick Mylar substrate material, containing 25,600 individual electrokinetic microactuators with 250-μm channel diameters arranged on 350-μm center-to-center spacings, as shown in Fig. 3 for full-scale hydronautical vehicle applications. These individual electrokinetic microactuators were grouped into 1600 individual unit-cells arranged in a 40×40 unit-cell pattern on each tile, with each unit-cell composed of a 4×4 array of microactuators. As shown in Fig. 9, every fifth row and column of microactuators in the tile was skipped to provide room for the resident unit-cell processing electronics. The top layer in Fig. 9 was fabricated by conventional MEMS processing steps.[37,38] The center layer was fabricated with the same porous polymer material in thin flexible Mylar substrate material suitable for conformal application on a vehicle surface.

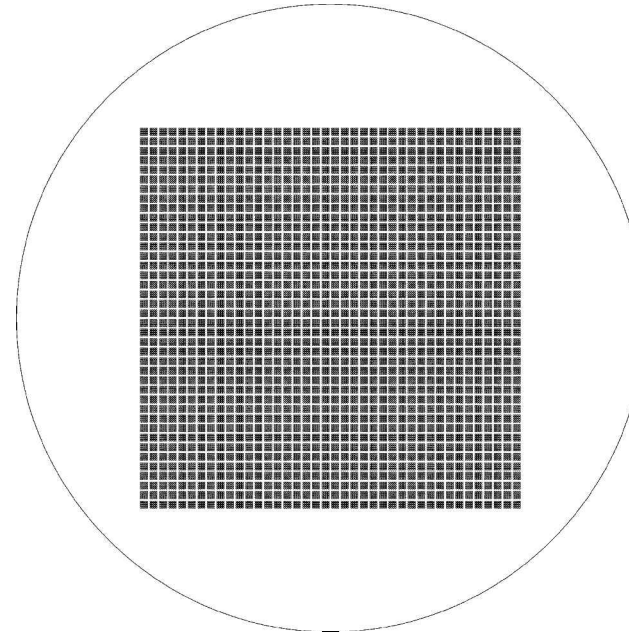

Fig. 8 Layout of electrokinetic microactuator channels in center layer of MEKA-5 full-scale hydronautical array, showing 25,600 individual microactuator channels grouped into a 40×40 pattern of unit-cells, each containing a 4×4 unit-cell structure on 325-μm center-to-center spacing.

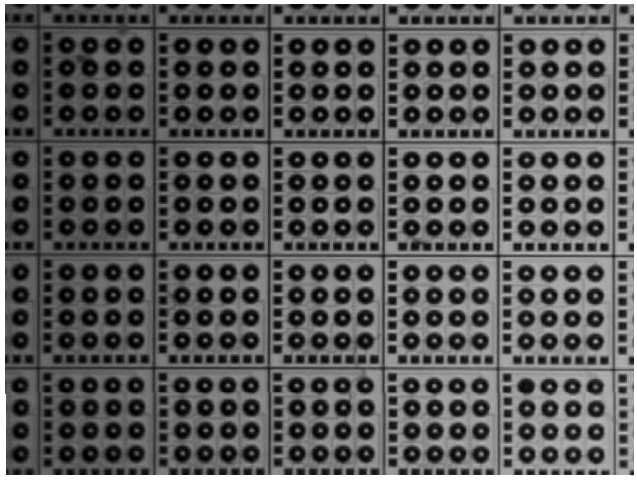

Fig. 9a Close-up view of the resulting unit-cell structure in the electrodes sublayer for the 25,600-element MEKA-5 hydronautical-scale array.

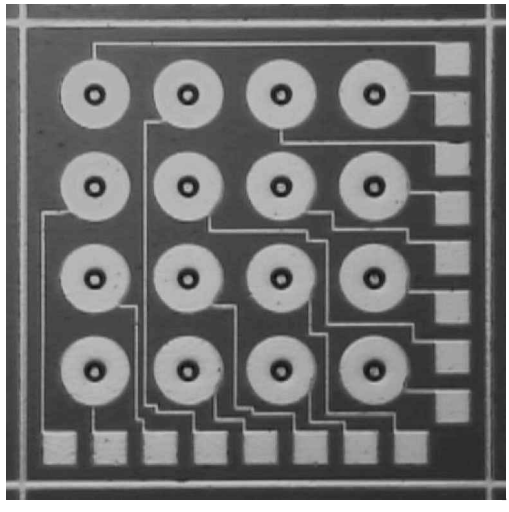

Fig. 9b Unit-cell-scale view of the electrodes sublayer, showing a single unit-cell.

DC performance testing of the electrokinetic flow rates produced by this porous polymer was conducted on the MEKA-1 actuator array. Various steady voltage differences ΔV were applied across the electrodes located in the top layer and the bottom layer and measuring the volume flow rate over an extended time. A complete description of the apparatus setup is given in Diez-Garias.[37] Results are shown in Fig. 10. The volume flow rate achieved was proportional to the applied voltage, consistent with relation (8), and for these conditions provided 0.1 ml/min at 15.3 V/mm. These results indicate that the 250-μm-diam electrokinetic actuators in the MEKA-5 array meet the 10 μl/min equivalent dc flow rate for hydronautical applications in Figs. 2 and 3 with applied voltages of 15–20 V across the 250-μm-thick center layer.

AC performance testing was also conducted to determine the frequency response by applying a sinusoidally time-varying voltage difference. These measurements were performed with a 1-mm-diam × 2-mm-thick polymer electrokinetic pump, driven by a function generator into a Burr–Brown 3745 high-voltage op-amp. The applied voltage was varied from 5 V peak to peak up to 90 V peak to peak. In this case the electrokinetic pump drove a small closed cavity containing an air bubble, and the time-varying pressure that developed in the cavity as the air bubble was compressed by the time-varying volume displacement achieved by the actuator was measured. A pressure transducer (Omega PX170-14GV) was used at low frequencies and a microphone (Brüel & Kjær 4138 microphone

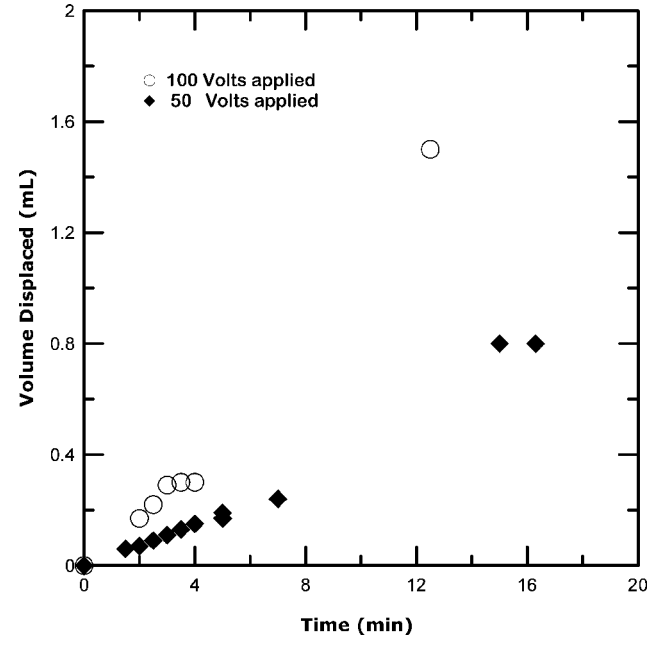

Fig. 10 Experimental results for steady electrokineic pumping performance achieved with MEKA-1 array for two different applied voltages. Total displaced volume increased linearly with time and varied with field strength.

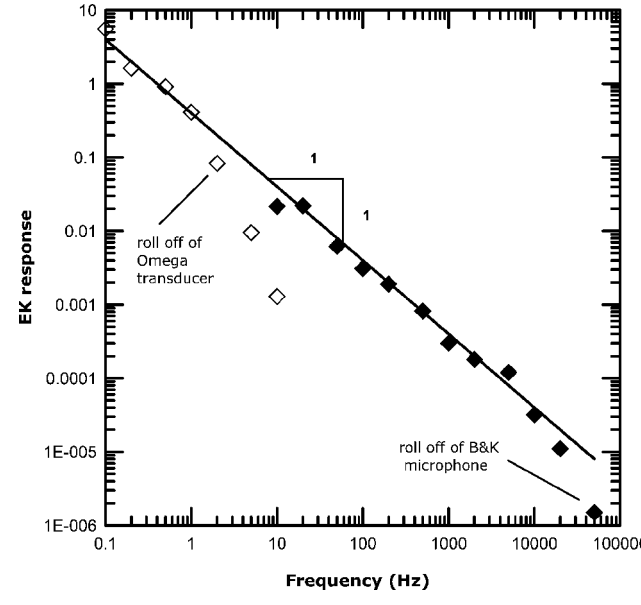

Fig. 11 Measured frequency response of an electrokinetic actuator for a sinusoidally time-varying applied field of various frequencies ω, showing results from a low-frequency pressure transducer and a high-frequency microphone: ——, f^{-1} roll-off corresponding to loss-less ac performance.

with B&K 2618 preamp) at high frequencies. Results are shown in Fig. 11, giving the relative peak-to-peak variation in the signal from the transducer or microphone normalized by the manufacturer's response calibration. The f^{-1} scaling shown by the solid line is the theoretical result corresponding to loss-less ac performance; i.e., the reduction in volume displacement per cycle resulting solely from the f^{-1} reduction in cycle period with frequency. The equivalent dc flow rate Q_{DC} is seen in Fig. 11 to be essentially constant up to applied frequencies at least as high as 10 kHz. The origins of the roll-off above 10 kHz remain unclear and may be due to an experimental limitation. The measured frequency at which this roll-off begins would be consistent with the onset of inertial damping in a

porous matrix structure with 10-μm pores, based on the considerations in Sec. IV.C, whereas the nominal pore size in the electrokinetic driver channels is believed to be about 1 μm. However, it is also possible that, whereas the pore size in the present matrix is nominally 1 μm, the largest pores can be as large as 10 μm and these determine the inertial damping limit for the actuator. Irrespective of these considerations, the 10-kHz frequency response demonstrated in these tests meets the demands for most of the vehicles in Figs. 2 and 3 and far exceeds the requirements for all of the hydronautical applications.

VI. Conclusions

The present study has been the first to examine the electrokinetic principle as the basis for a new class of microscale actuator arrays for active sublayer control on full-scale aeronautical and hydronautical vehicles under realistic operating conditions. Specific performance requirements for microactuator spacing, flow rate, and frequency response for active sublayer control have been determined from fundamental scaling laws for the streamwise vortical structures in the sublayer of turbulent boundary layers.

In view of the inherently local nature of the sublayer dynamics, a general system architecture for microactuator arrays appropriate for active sublayer control has been developed based on the concept of relatively small and independent unit-cells, each with their own sensing, processing, and actuation capability, which greatly simplifies the sensing and processing requirements needed to achieve practical sublayer control. A fundamental three-layer design has been developed for such electrokinetic microactuator arrays, in which electrokinetic flow is induced by an impulsively applied electric field across a center layer, with a bottom layer containing an electrolyte reservoir and a common electrode, and a top layer that contains individual electrodes and lead-outs for each microactuator in the unit-cell.

A recently developed porous polymer fabrication technology has been adapted to permit formation of fine-pore matrix structures suitable for electrokinetic pumping in large, dense arrays of microchannels. Measured volume flow rates under the effect of steady applied electric fields have been shown to meet the requirements for active sublayer control on full-scale vehicles. The thin layers into which these electrokinetic microactuators can be fabricated permits the required field strengths to be achieved with potential differences of the order of 15–20 V. Measurements of the actual frequency response achieved in such electrokinetic actuators have verified essentially loss-less ac performance at frequencies as high as 10 kHz.

Several generations of such electrokinetic microactuator arrays have been built leading to the MEKA-5 full-scale hydronautical array, composed of 25,600 individual electrokinetic microactuators with 350-μm center-to-center spacings, arranged in a 40×40 pattern of unit-cells, each composed of a 4×4 matrix of actuators. This array was successfully fabricated in a 7×7 cm^2 tile in 250-μm-thick Mylar substrate material.

Acknowledgments

This work was supported by the Defense Advanced Research Projects Agency (DARPA) MEMS/MTO Program under Contract F30602-98-2-0228. The assistance of Phillip H. Paul and Ken R. Hencken of the Microtechnology Department at Sandia National Laboratories in fabrication and testing of the electrokinetic microactuators is gratefully acknowledged, as is the assistance of Khalil Najafi and Paul Sunal at the University of Michigan MEMS Exchange in fabricating the MEKA-5 array.

References

[1]Dahm, W. J. A., Paul, P. H., Rakestraw, D. J., and Scherer, J. J., "Fluid Microactuators Based on the Electrokinetic Principle," *Bulletin of the American Physical Society*, Vol. 42, 1997, p. 2247 (abstract only).

[2]Diez-Garias, F. J., Dahm, W. J. A., and Paul, P. H., "Microactuator Arrays for Sublayer Control in Turbulent Boundary Layers Using the Electrokinetic Principle," AIAA Paper 2000-0548, Jan. 2000.

[3]Dahm, W. J. A., and Diez-Garias, F. J., "Electrokinetic Microactuator Arrays for Sublayer Control in Turbulent Boundary Layers," *Proceedings of the 2nd International Symposium on Smart Control of Turbulence*, edited by N. Kasagi, Univ. of Tokyo, Tokyo, 2001, pp. 107–116.

[4]Kline, S. J., Reynolds, W. C., Schraub, F. A., and Runstadler, P. W., "The Structure of Turbulent Boundary Layers," *Journal of Fluid Mechanics*, Vol. 30, 1967, pp. 741–773.

[5]Kim, H. T., Kline, S. J., and Reynolds, W. C., "The Production of Turbulence near a Smooth Wall in a Turbulent Boundary Layer," *Journal of Fluid Mechanics*, Vol. 50, 1971, pp. 133–168.

[6]Robinson, S. K., "Coherent Motion in the Turbulent Boundary Layer," *Annual Review of Fluid Mechanics*, Vol. 23, 1991, pp. 601–639.

[7]Chara, Z., Zakin, J. L., and Myska, S. J., "Turbulence Measurements of Drag Reducing Surfactant Systems," *Experiments in Fluids*, Vol. 16, 1993, pp. 36–41.

[8]Myska, J., Zakin, J. L., and Chara, Z., "Viscoelasticity of a Surfactant and It's Drag Reducing Ability," *Applied Scientific Research*, Vol. 55, 1995, pp. 297–310.

[9]Warholic, M. D., Schmidt, G. M., and Hanratty, T. J., "The Influence of a Drag Reducing Surfactant on a Turbulent Velocity Field," *Journal of Fluid Mechanics*, Vol. 388, 1999, pp. 1–20.

[10]Zakin, J. L., and Qi, Y., "Some Recent Developments in Surfactant Drag Reduction," *Proceedings of the 2nd Symposium on Smart Control of Turbulence*, Univ. of Tokyo, Tokyo, 2001, pp. 43–58.

[11]Choi, K.-S., "Near-Wall Structure of a Turbulent Boundary Layer with Riblets," *Journal of Fluid Mechanics*, Vol. 208, 1989, pp. 417–458.

[12]Choi, K.-S., "Turbulent Structure Revisited; Results and Implications from Riblets Research," *Near Wall Turbulent Flows*, edited by R. M. C. So, C. G. Speziale, and B. E. Launder, Elsevier, New York, 1993, pp. 699–707.

[13]Choi, H., Moin, P., and Kim, J., "Direct Numerical Simulation of Turbulent Flow over Riblets," *Journal of Fluid Mechanics*, Vol. 255, 1993, pp. 503–539.

[14]Pollard, A., "Passive and Active Control of Near-Wall Turbulence," *Progress in Aerospace Sciences*, Vol. 33, 1997, pp. 689–708.

[15]Breuer, K. S., Haritonidis, J. H., and Landahl, M., "The Control of Transient Disturbances in a Flat Plate Boundary Layer Through Active Wall Motion," *Physics of Fluids A*, Vol. 1, 1989, pp. 574–582.

[16]Nosenchuck, D. M., and Brown, G. L., "Discrete Spatial Control of a Wall Shear Stress in a Turbulent Boundary Layer," *Near Wall Turbulent Flows*, edited by R. M. C. So, C. G. Speziale, and B. E. Launder, Elsevier, New York, 1993.

[17]Wilkinson, S. P., "Interactive Wall Turbulence Control," *Viscous Drag Reduction in Boundary Layers*, edited by D. M. Bushnel and J. N. Hefner, Vol. 123, Progress in Astronautics and Aeronautics, AIAA, Washington, DC, 1990, pp. 479–509.

[18]Gad-el-Hak, M., "Flow Control," *Applied Mechanics Reviews*, Vol. 42, 1989, pp. 261–293.

[19]Gad-el-Hak, M., "Interactive Control of Turbulent Boundary Layers: A Futuristic Overview," *AIAA Journal*, Vol. 32, 1994, pp. 1753–1765.

[20]Gad-el-Hak, M., "Modern Developments in Flow Control," *Applied Mechanics Reviews*, Vol. 49, 1996, pp. 365–379.

[21]Gad-el-Hak, M., "Flow Control: the Future," *Journal of Aircraft*, Vol. 38, 2001, pp. 402–418.

[22]Choi, H., Moin, P., and Kim, J., "Active Turbulence Control for Drag Reduction in Wall-Bounded Flows," *Journal of Fluid Mechanics*, Vol. 262, 1994, pp. 75–110.

[23]Moin, P., and Bewley, T., "Feedback Control of Turbulence," *Applied Mechanics Reviews*, Vol. 47, 1994, pp. S3–S13.

[24]Ho, C.-M., and Tai, Y.-C., "Micro-Electro-Mechanical-Systems (MEMS) and Fluid Flows," *Annual Review of Fluid Mechanics*, Vol. 30, 1998, pp. 579–612.

[25]Lumley, J. L., and Blossey, P., "Control of Turbulence," *Annual Review of Fluid Mechanics*, Vol. 30, 1998, pp. 311–327.

[26]Löfdahl, L., and Gad-el-Hak, M., "MEMS Applications in Turbulence and Flow Control," *Progress in Aerospace Science*, Vol. 35, 1999, pp. 101–203.

[27]Rebbeck, H., and Choi, K.-S., "Opposition Control of Near-Wall Turbulence with a Piston-Type Actuator," *Physics of Fluids*, Vol. 13, 2001, pp. 2142–2145.

[28]Gad-el-Hak, M., *Flow Control: Passive, Active, and Reactive Flow Management*. Cambridge Univ. Press, New York, 2000.

[29]Hammond, E. P., Bewley, T. R., and Moin, P., "Observed Mechanisms for Turbulence Attenuation and Enhancement in Opposition-Controlled Wall-Bounded Flows," *Physics of Fluids*, Vol. 10, 1998, pp. 2421–2423.

[30]Reuss, F. F., Sur un Nouvel Effet de l'Éctricité Galvanique," *Memoires de la Societé Imperiale de Naturalistes de Moscou*, Vol. 2, 1809, pp. 327–337.

[31]Potter, E. C., *Electrochemistry, Principles and Applications*, Cleaver-Hume, London, 1961.

[32]Burgreen, D., and Nakache, F. R., "Electrokinetic Flow in Ultrafine Capillary Slits," *Journal of Physical Chemistry*, Vol. 68, 1964, pp. 1084–1091.

[33]Rice, C. L., and Whitehead, R., "Electrokinetic Flow in a Narrow Cylindrical Capillary," *Journal of Physical Chemistry*, Vol. 69, 1965, pp. 4017–4023.

[34]Overbeek, J. Th. G., and Wiersema, P. H., *Electrophoresis*, Academic Press, New York, 1967.

[35]Peters, E. C., Petro, M., Svec, F., and Fréchet, J. M. J., "Molded Rigid Polymer Monoliths as Separation Media for Capillary Electrochromatography. 1. Fine Control of Porous Properties and Surface Chemistry," *Analytical Chemistry*, Vol. 70, 1998, pp. 2288–2295.

[36]Peters, E. C., Petro, M., Svec, F., and Fréchet, J. M. J., "Molded Rigid Polymer Monoliths as Separation Media for Capillary Electrochromatography. 2. Effect of Chromatographic Conditions on the Separation," *Analytical Chemistry*, Vol. 70. 1998, pp. 2296–2302.

[37]Diez-Garias, F. J., "Electrokinetic Microactuator Arrays for Active Sublayer Control of Turbulent Boundary Layers," Ph.D. Dissertation, Dept. of Aerospace Engineering, Univ. of Michigan, Ann Arbor, MI, April 2002.

[38]Diez, F. J., and Dahm, W. J. A., "Micro Electro Kinetic Actuator (MEKA) Arrays for Active Sublayer Control of Turbulent Boundary Layers," AIAA Paper 2002-0267, Jan. 2002.

R. M. C. So
Associate Editor